General Disclaimer

One or more of the Following Statements may affect this Document

- This document has been reproduced from the best copy furnished by the organizational source. It is being released in the interest of making available as much information as possible.

- This document may contain data, which exceeds the sheet parameters. It was furnished in this condition by the organizational source and is the best copy available.

- This document may contain tone-on-tone or color graphs, charts and/or pictures, which have been reproduced in black and white.

- This document is paginated as submitted by the original source.

- Portions of this document are not fully legible due to the historical nature of some of the material. However, it is the best reproduction available from the original submission.

SOLAR SATELLITE PROJECT

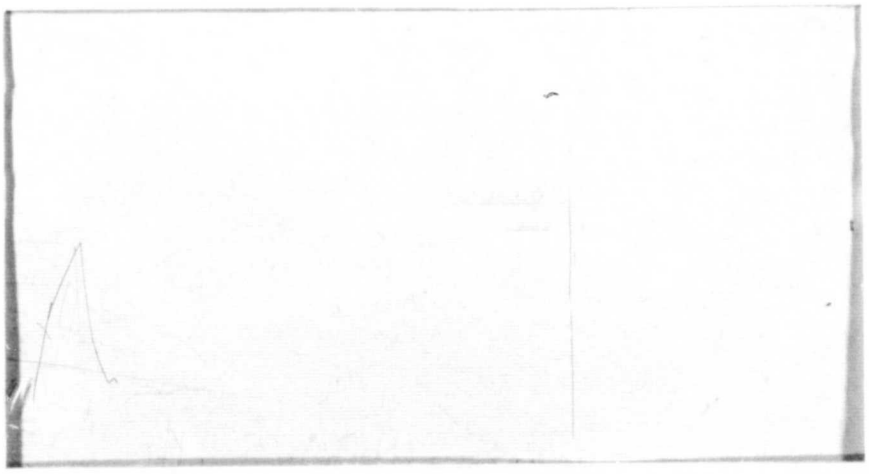

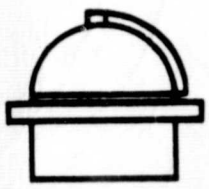

HARVARD COLLEGE
OBSERVATORY

60 GARDEN STREET

CAMBRIDGE, MASS

25

ORBITAL PLASMA TESTS

for

HARVARD OSO-D EXPERIMENT

Technical Report No. 8

NASA Contract No. NASw-184

May 1969

By Stanley M. Diamond

ABSTRACT

A test was conducted by the Harvard College Observatory to investigate the effect of orbital plasma on the operation and performance of the HCO Experiment for the NASA spacecraft OSO-D. Another objective was to determine an optimum ion grid configuration to reduce the plasma entering the outer covers of the experiment. The test was conducted by installing the experiment in a simulated space environment and recording the effects of different plasma environments on the system performance. The tests showed that orbital plasma does not detract from the performance of the HCO Experiment and does not induce any high voltage discharge during its operation.

TABLE OF CONTENTS

TABLE OF CONTENTS

LIST OF APPENDIXES

LIST OF APPENDIXES

LIST OF ILLUSTRATIONS

LIST OF TABLES

List of Tables

1.0 INTRODUCTION

This report discusses an orbital plasma test performed on the Harvard College Observatory (HCO) Experiment for the NASA spacecraft OSO-D. The test was conducted at the NASA Goddard Space Flight Center (GSFC), Greenbelt, Maryland, from November 21, 1966, to December 19, 1966.

Knowing how orbital plasma effects the operation of the HCO Experiment is of vital importance because inadequate immunity to plasma could cause high voltage breakdowns and thereby unsatisfactory performance of the instrument. Moreover, because the windowless photomultipliers used in the HCO Experiment are sensitive to charged particles, the desired ultraviolet flux data would be indistinguishable from the spurious data associated with the incident plasma flux.

The test had two objectives: a) to find how orbital plasma affects the operation of the HCO spectrometer; b) to determine an optimum ion grid configuration (including the grid voltages) for various plasma environments.

2.0 HCO EXPERIMENT

The function of the HCO Experiment in the OSO-D is to map the intensities of solar radiation in the wavelength region 300Å through 1300Å of the extreme ultraviolet.

2.1 OPTICAL ARRANGEMENT

The optical arrangement of the HCO Experiment is illustrated in Figure 1. Parallel light rays from the sun enter through the entrance aperture, travel the length of the instrument and strike the telescope mirror. This is a spherical platinum coated mirror 4 cm square with a 50 cm focal length (f/12.5). The entrance slit S is 150μm x 150 μm and is located at the primary focus of the collecting mirror. This slit is the instrument field stop and defines the system field of view (arc tan 150 μm/50 cm ≈ 1 arc min).

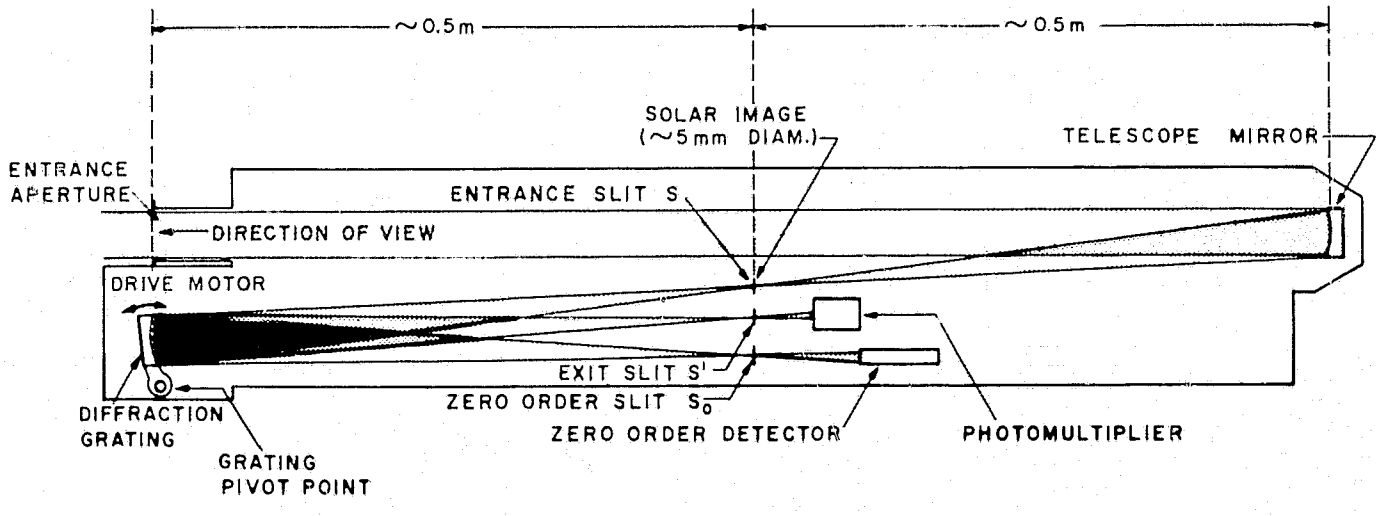

Fig. 1 – HARVARD OSO-G1 OPTICAL LAYOUT

Light from a 1 x 1 arc minute element of the solar disc passes through entrance slit S and strikes the diffraction grating. This grating is a Bausch & Lomb original ruled 1800 lines/mm in gold. The ruled area measures 4 cm x 4 cm, and has a radius of curvature of 50 cm (f/12.5) and an 850Å first-order blaze. Exit slit S' is 300 μm wide x 1000 μm. This dimension broadens the wavelength resolution to 3.6Å without affecting the field-stop properties of the entrance slit.

A Johnson Onaka mounting of near normal incidence is used for the grating. Light from the entrance slit is diffracted by the grating to form a series of dispersed images with positions that are a function of wavelength. Successive images in the series are indexed onto the exit slit by rotating the grating angle in discrete steps (Wavelength Scan Mode); or a particular wavelength is selected for analysis by stopping the grating at the appropriate angular position (Raster Mode).

As the grating angle changes, light from successive spectral emission lines passes through the exit slit S', and strikes the cathode of the photomultiplier. This device is an open, crossed electric and magnetic field, electron multiplier (Bendix Model 310) with a tungsten photocathode and a distributed resistance dynode strip which requires a potential of approximately 1800 volts. An open photomultiplier is used because no envelope or

window material will pass ultraviolet (UV) radiation below the 1050Å cutoff of lithium flouride. The tungsten photocathode has a relatively high work function. This characteristic prevents the photomultiplier from detecting longer wavelength radiation (visible and infra-red) and thus degrading the signal-to-noise ratio. In the extreme UV regions, the low intensities of solar radiation make it necessary to employ measuring methods that depend upon the count of individual photons rather than on conventional photomultiplier averaging techniques.

Photons incident upon the photomultiplier yield output pulses that are coupled to a detection circuit which consists of a pre-amplifier, pulse amplifier, and a binary counter.

2.2 EXTERNAL APPEARANCE

The external appearance of the HCO Experiment is shown in Figure 2. A view of the same experiment with its dust covers removed is contained in Figure 3.

2.3 ION GRIDS

Seven ion grids and a mirror ring are installed at appropriate points in the HCO Experiment to reduce the effect of charged particles on the performance of the instrument. The ion grids are silver-plated screens (0.0005 inch thick with 90 percent optical transmission) mounted

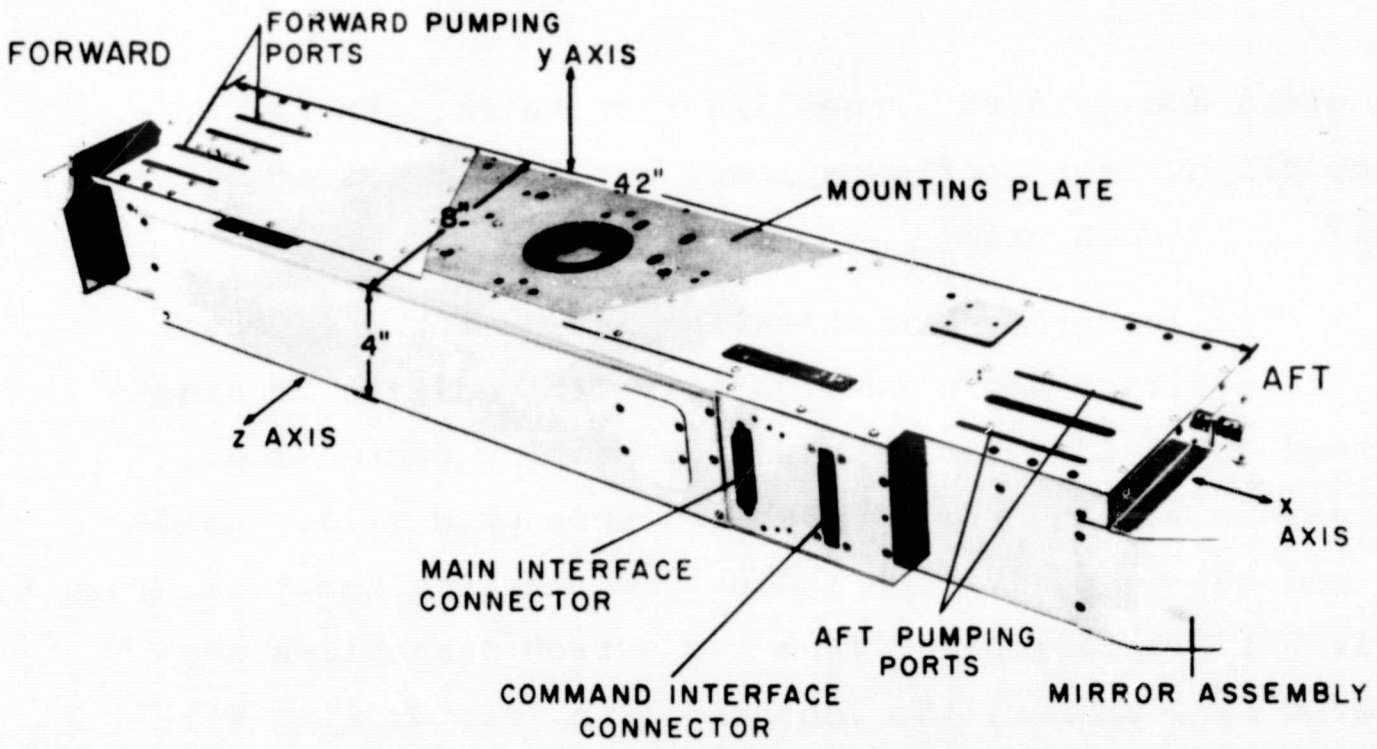

FIGURE 2

EXTERNAL APPEARANCE OF HCO EXPERIMENT WITH DUST COVER INSTALLED

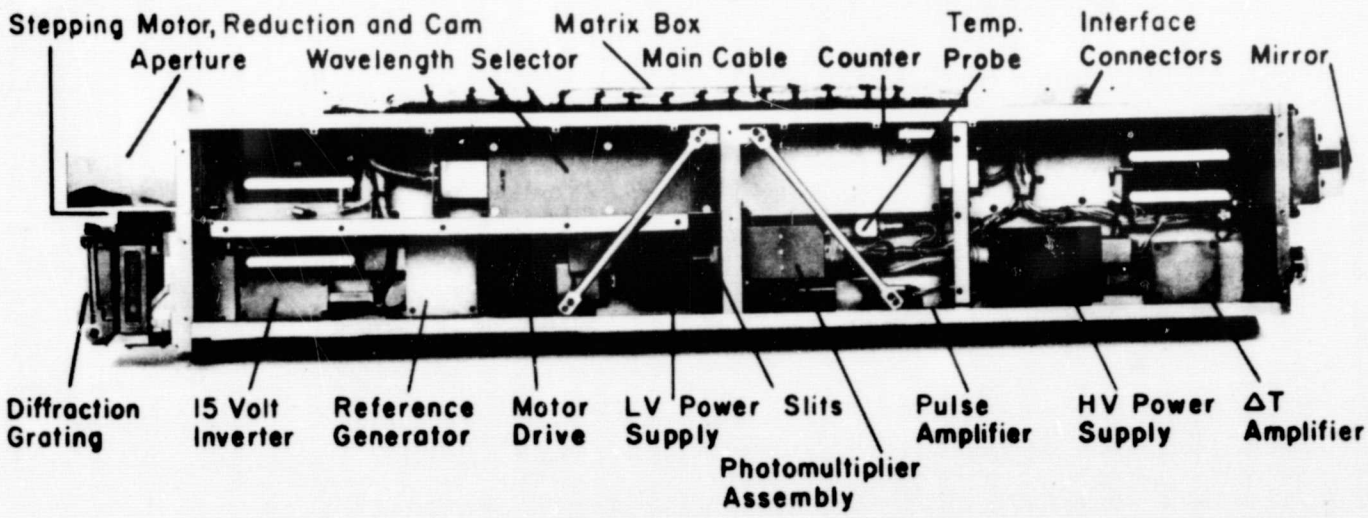

FIGURE 3

APPEARANCE OF HCO EXPERIMENT WITHOUT DUST COVER

on glass epoxy-board frames 1/8 inch thick. In the present flight/test configurations, a +15 volt potential is applied to each grid.

The ion grids are installed inside the dust cover in the position shown in Figure 4. In addition to single screen grids installed inside the pumping ports (i.e., grids #3, #5, and #6), a double screen grid (i.e., grids #7 and #8) is positioned inside the entrance aperture. (Fig. 5) This grid is fabricated from two screen assemblies separated by a spacer. An ion ring (i.e. mirror ring #4) is also installed in front of the mirror assembly to suppress secondary electrons from the mirror. Grids #3, #5, #6, #7, and #8, and ring #4 are installed in the present flight/test configurations. The single-screen grid (i.e. grid #9) at the snout entrance aperture was installed for test purposes only.

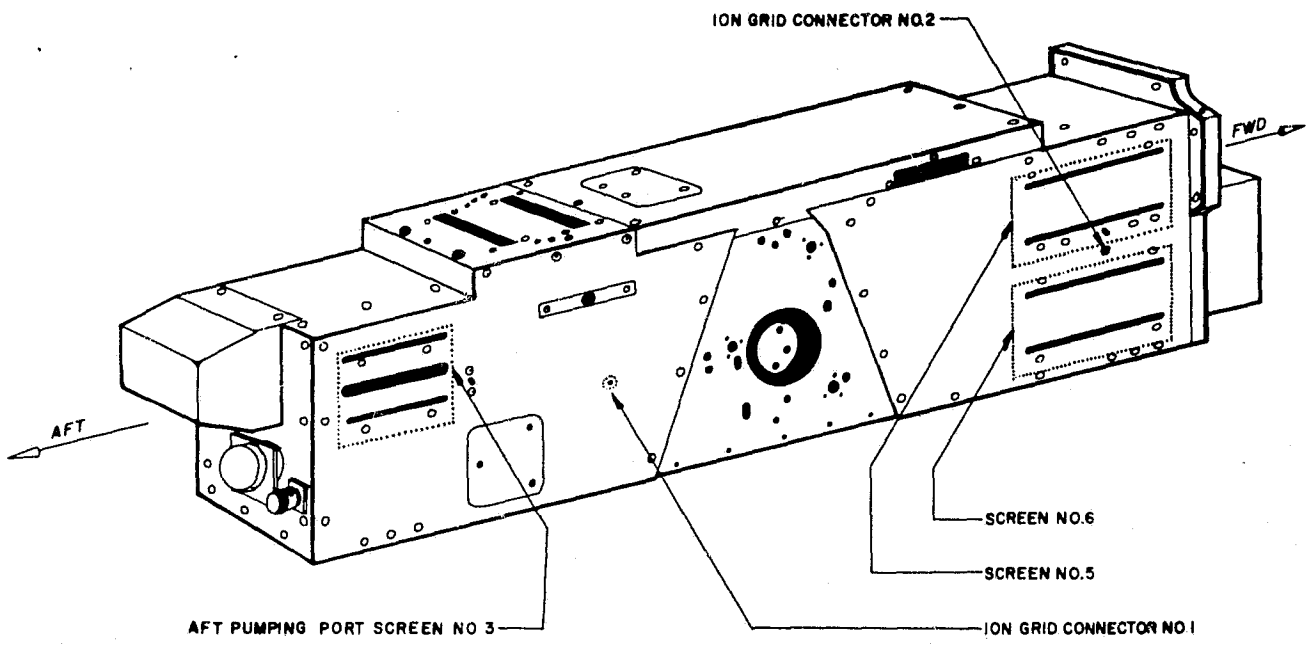

ION GRID SCREENS AND CONNECTORS ON RIGHT SIDE OF DUST COVER

FIGURE 4

ION GRID SCREENS AND PROBES ON THE LEFT SIDE OF THE DUST COVER

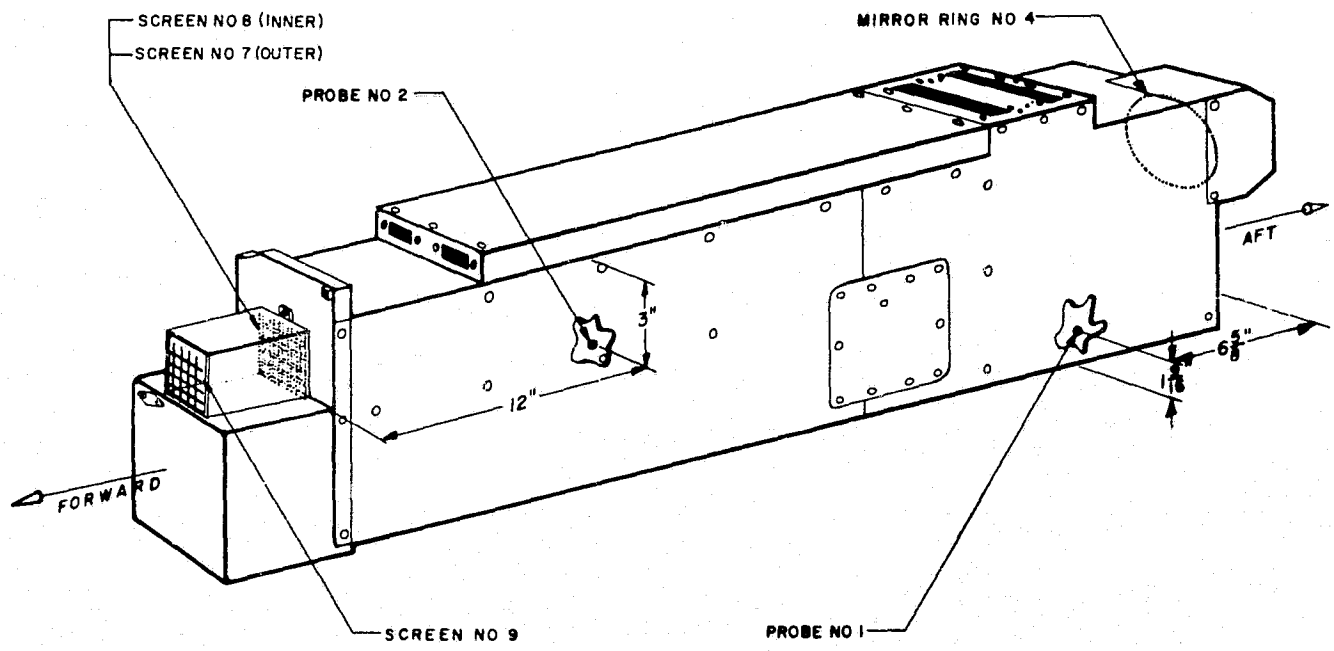

FIGURE 5

LOCATIONS OF ION GRID SCREENS, ION GRID CONNECTORS AND PROBES ON DUST COVER

3.0 TEST FACILITY

3.1 SIMULATED SPACE PLASMA ENVIRONMENT

The orbital plasma test was performed by installing the HCO Experiment in a simulated space environment and investigating how the different environmental conditions affect the behavior of the UV detection system. Simulated space environments were produced in a GSFC vacuum chamber equipped with both a hydrogen UV source and a plasma source. The UV source provided a means for checking the detection system after different environmental conditions had been established. Plasma densities of 10^4 to 10^6 particles/cm^3 were generated by a system consisting of a hot filament electron source, a set of accelerating plates and a flow of nitrogen molecules (cf. Figure 6).

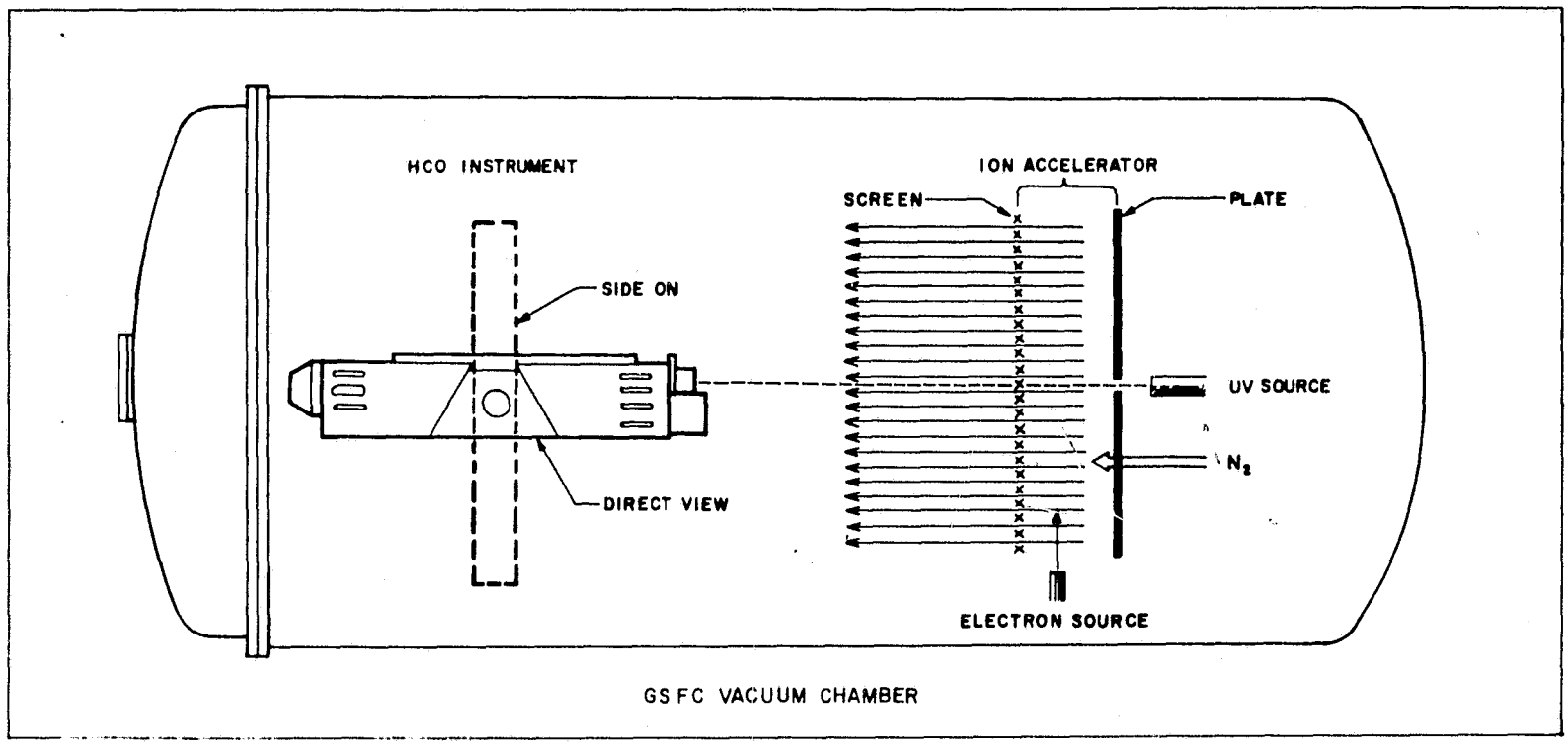

FIGURE 6
PLASMA TEST ARRANGEMENT
(OPTICAL AXIS PARALLEL TO PLASMA FLOW VECTOR)

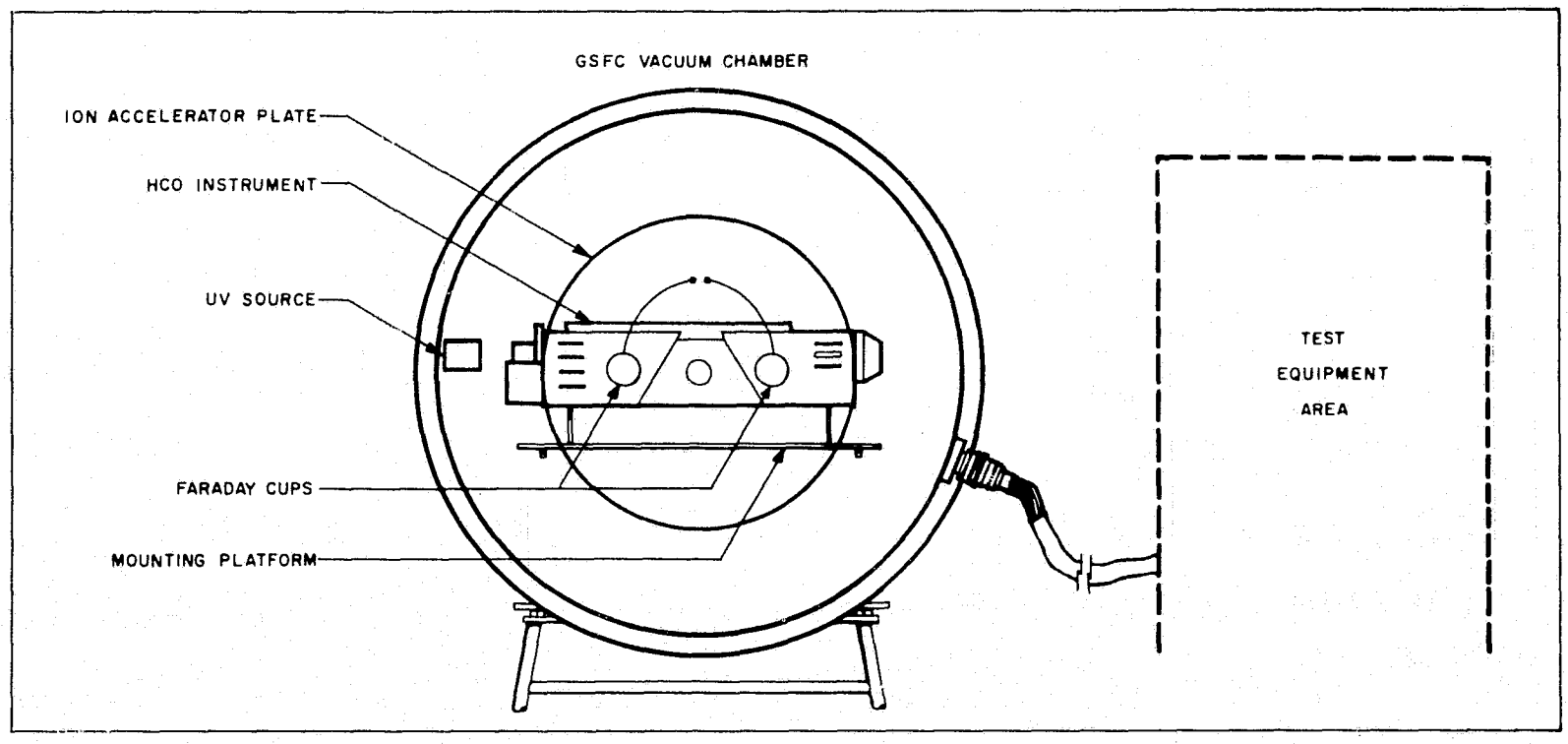

FIGURE 7
HCO EXPERIMENT MOUNTED IN GSFC THERMAL VACUUM CHAMBER WITH
OPTICAL AXIS PERPENDICULAR TO THE PLASMA FLOW VECTOR

The simulated environment used in the test was provided by a GSFC (Goddard Space Flight Center) test facility developed by D. R. Burrowbridge, Function Test Branch, GSFC. This facility consists of a thermal vacuum chamber equipped with a UV source, a plasma source, and ion accelerator and an adjustable support to hold the HCO Experiment. The thermal vacuum chamber is a steel cylinder (7 feet in diameter, 8 feet in length) with bell-shaped ends. One end is welded to the cylindrical body, the other is removeable and is fitted with a circular glass window (cf. Figures 6 and 7).

Plasma simulation is produced by a beam of high energy electrons emitted from a hot filament source and accelerated between a set of circular and parallel grid plate elements. These elements have a diameter of 48 inches and are separated by a distance of 8 inches. Fittings are provided to install the 1216Å UV source in an appropriate position for exciting the HCO Experiment. A normal tubular ionization gauge is installed in the chamber wall to monitor the chamber pressure, and an open ionization gauge at the plasma source monitors the local pressure at the source. The source pressure can be varied to control the ion flux. For this purpose, gaseous N^2 is introduced through a variable leak valve with a minimum leak rate of approximately 1×10^{-8} standard cc/sec.

Connector pads are installed on the chamber to provide for transfer of appropriate signals between the HCO Experiment and the external test equipment. A block diagram of this test equipment is shown in Figure 8.

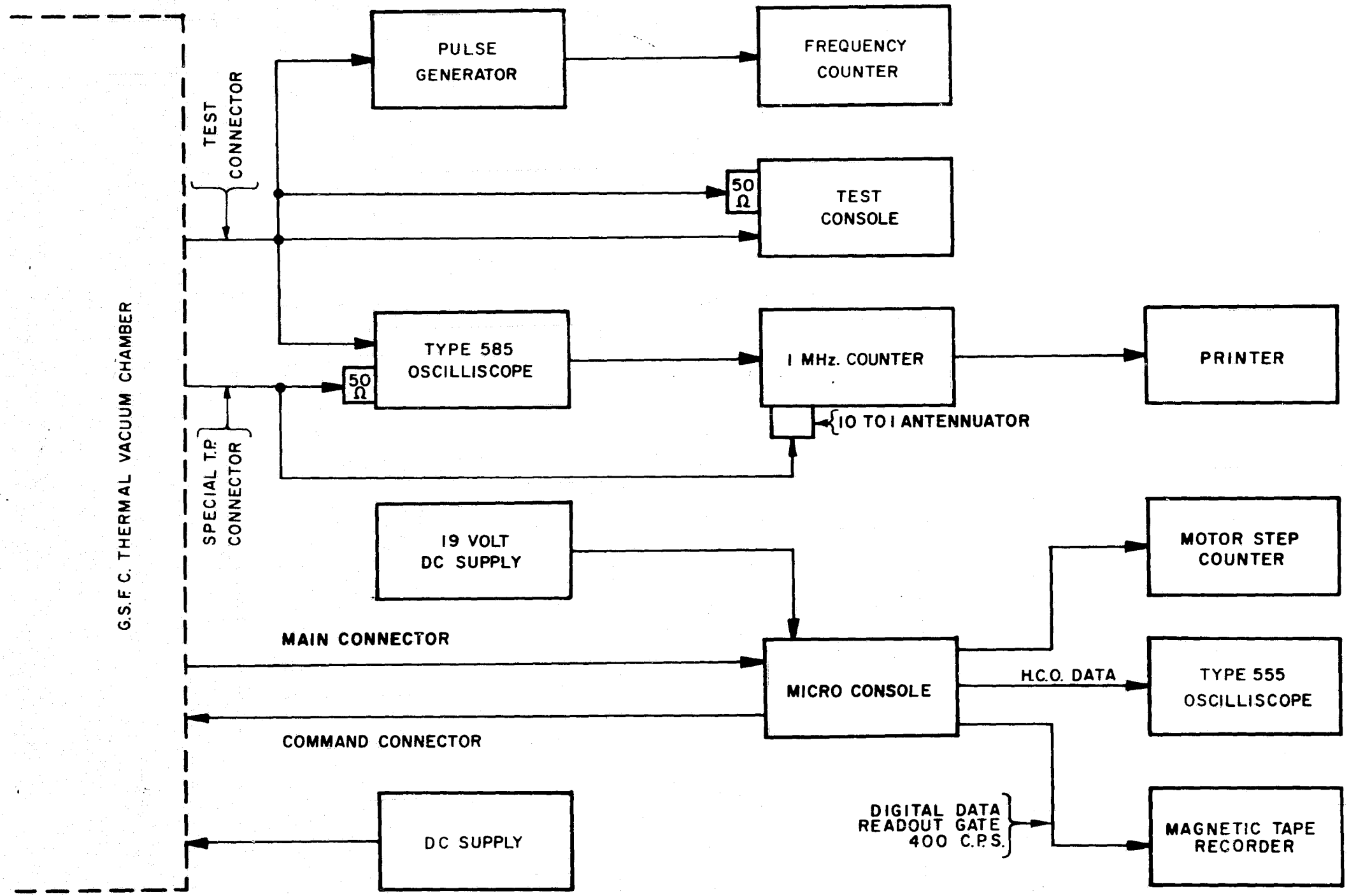

TEST EQUIPMENT FOR ORBITAL PLASMA TEST

FIGURE 8.

3.2 AVAILABLE ENVIRONMENTAL CONDITIONS

The environmental conditions available in the above GSFC Test Facility are as follows:

A.	Density (Electrons and/or positive ions)	2×10^4 to 2×10^6 particles/cm^3
B.	Flux (Flux = density x orbital velocity)	$\geq 2 \times 10^5$ particles/cm^3 x 7×10^5 cm/sec $\geq 1.4 \times 10^{11}$ particles/cm^2/sec
C.	Flux range	1.4×10^{10} to 1.4×10^{12} particles/cm^2/sec
D.	UV Source	1216Å
E.	Temperature	Room ambient (25°C)

3.3 TEST CONFIGURATION

To simulate the plasma conditions encountered during flight, the HCO Experiment was oriented in the vacuum chamber in two different directions with respect to the plasma flow.

One set of plasma conditions simulated those encountered when the HCO Experiment is pointing at the sun. For this simulation the HCO Experiment was installed in the vacuum chamber with its optical axis pointed parallel to the plasma flow vector (cf. Figure 6) and with the UV source

mounted behind the flat plate of the ion accelerator.

Another set of plasma conditions simulated those encountered when the HCO Experiment is pointing approximately perpendicular to the direction of flight. For this simulation the HCO Experiment was rotated through 90 degrees so that its optical axis was pointed towards a UV source near the left wall of the chamber (cf Figure 7). Because orientation of the ion accelerator remained the same, the optical axis was perpendicluar to the plasma flow vector.

3.4 DENSITY AND FLUX MEASUREMENTS

Plasma density was measured during the tests by two probes attached to the inside of the dust cover (cf. Figure 5). Ion flux measurements outside of the dust cover were made with two Faraday cups suspended from the ion accelerator. These cups were placed about 20 inches apart in the plane of the optical axis and in the locations shown in Figures 6 and 7. In one phase of the test, a Faraday cup and a probe were installed at a position inside of grids #7 and #8 to measure the ion and electron flux energies at the entrance aperture (cf. Figure 5).

4.0 TEST PHASES

This section discusses the test methods and the results for each of the four phases of the orbital plasma test.

4.1 PHASE I - EFFECT OF PLASMA ON FLIGHT CONFIGURATION

The object of Phase I was to determine how orbital plasma affects the performance of the flight configuration of the HCO Experiment (hereafter called the "instrument"). The test method consisted of recording the output count of the instrument under different plasma conditions, and of simultaneously observing the output waveform on an oscilloscope. Readings were taken with the high voltage supply of the detection system turned on and the UV source turned on and off.

The instrument performance when no plasma was applied was checked before and after each test sequence. Hence the variation in the output count from test to test was an indication of the effect of plasma degraded or enhanced on the performance of the detection system.

A sequence of tests was conducted for each test configuration described in Section 3.3. Different plasma densities were used for each test so that every sequence covered a specific range of plasma densities.

4.1.1 INSTRUMENT ORIENTED PARALLEL TO PLASMA FLOW VECTOR

Table I summarizes the results obtained for the test sequence conducted when the optical axis of the instrument was oriented parallel to the plasma flow vector. Runs were made with the plasma switched from the lowest possible value to the highest possible intensity (cf. Table I).

4.1.2 INSTRUMENT ORIENTED NORMAL TO PLASMA FLOW VECTOR

Table II summarizes the results obtained when the instrument was directed normal to the plasma flow. The other conditions were the same as those used in the test sequence of Section 4.1.1.

4.1.3 DISCUSSION OF PHASE I RESULTS

The results summarized in Tables I and II indicate that orbital plasma would not seriously degrade the performance of the flight configuration of the HCO Experiment. This deduction does not imply that the flight configuration is completely immune to the effects of plasma. However, even with the highest possible flux, the output noise level was below any level that would detract from the instrument's ability to acquire data. The only noticeable effect of plasma was a burst of pulses that occurred at the Turn-on of the instrument in a plasma environment. These turn-on transients however were of short duration (i.e., less than two seconds) and their

TABLE X

TEST DATA - PHASE I WITH OPTICAL AXIS OF INSTRUMENT ORIENTED PARALLEL TO PLASMA FLOW VECTOR

Test Conditions

a. Plasma switched from lowest possible level to highest possible intensity

b. Ion grid voltages of +15V supplied from internal source

c. HV on

Test No.	Vacuum Pressure (mm/Hg)	Plasma flux (particles/ cm^2/second)	UV Source	Comment
1	3.0×10^{-6}	None	—	Noise check, HV primary current 8 ma. No. significant counts. System reasonably quiet.
2	9.0×10^{-6}	None	ON	Counts lower by a factor of 4 than previous test.
3	9.0×10^{-6}	6.0×10^{9}	OFF	No appreciable counts when HV turned on. Instrument at MECHANICAL REFERENCE plasma at lowest possible intensity, i.e. 50% >9ev.
4	9.8×10^{-6}	6.0×10^{9}	ON	Counts recorded.
5	3.3×10^{-5}	6.0×10^{10}	ON	Low counts.
6	3.2×10^{-5}	6.0×10^{10}	ON	
7	4.5×10^{-5}	1.8×10^{11}	OFF	50% below 3 ev.
8	4.5×10^{-5}	1.8×10^{11}	ON	Very high counts.
9	4.5×10^{-5}	1.8×10^{11}	ON	HV primary current slightly higher than test #8, i.e., 8.2 ma. Increased to 8.9 ma as test continues.
			OFF	—
10	5.0×10^{-5}	1.8×10^{11}	OFF	HV primary current 8.8 ma.
11	5.0×10^{-5}		OFF	Electron flux at start was 40 $\mu A/cm^2$ HV primary current 8.4 ma.
12	4.2×10^{-5}	1.8×10^{11}	OFF	Maximum plasma density, i.e. 50% <4.5 ev. HV primary current 8.2 ma.
13	4.6×10^{-5}	3.0×10^{11}	OFF	Absolute maximum possible + ions i.e., 50% below 2 ev. HV primary current 8.2 ma. cycled HV on and off 3 times.
14	5.0×10^{-5}	3.0×10^{11}	ON	

TABLE II

TEST DATA - PHASE I WITH OPTICAL AXIS

OF INSTRUMENT ORIENTED NORMAL TO PLASMA FLOW VECTOR

TEST CONDITIONS

a. Plasma at different densities switched on and off.

b. Ion grid voltages of +15V supplied by internal source.

c. HV on.

Test No.	Vacuum Pressure (mm/Hg)	Plasma Density I+ - part/cm^3 I- - amp/cm^2	UV Source	Comment
1	1×10^{-6}	2×10^{-9} amp/cm^2	OFF	No significant noise count.
2	3×10^{-5}	5×10^{5} part/cm^3	OFF	
3	3.6×10^{-5}	5×10^{5} part/cm^3	ON	System operates properly.
4	4.3×10^{-5}	1×10^{6} part/cm^3	OFF	No significant noise count.
5	4.4×10^{-5}	1×10^{6} part/cm^3	OFF	
6	4.3×10^{-5}	1×10^{6} part/cm^3 2×10^{-5} amp/cm^2	ON	System operates properly.
7	4.9×10^{-5}	5×10^{-5} amp/cm^2	OFF	No significant noise count.
8	4.3×10^{-5}	5×10^{-5} amp/cm^2	ON	System operates properly.

maximum output count was usually lower than 100. Transients having these characteristics were observed throughout all test phases but were considered acceptable because they disappeared after a very short period of time.

4.2 PHASE II - EFFECT OF DIFFERENT GRID VOLTAGES ON PLASMA REDUCTION

The objective of Phase II was to determine the optimum grid voltages for the ion grids and the mirror rings of the instrument.

The instrument tested in Phase II had the same configuration as the one described in Phase I, except that two internal probes and the snout grid, #9, were added. Also, external DC voltages were applied through ion grid connections #1 and #2 (cf. Figure 4). These external voltages were distributed inside the instrument to the ion grids used during each run. In subsequent paragraphs and tables the ion grids and the mirror ring are designated by the numerals in Figure 4 .

4.2.1 TEST SEQUENCES WITH OPTICAL AXIS OF THE INSTRUMENT PARALLEL TO THE PLASMA FLOW VECTORS

In two test sequences the optical axis of the instrument was directed parallel to the plasma flow vector. In one sequence the grids (including snout grid #9) were connected internally so that the voltage listed in Table III

TABLE III
PHASE II, PART I
EFFECTS OF DIFFERENT ENTRANCE GRID VOLTAGES WITH THE OPTICAL AXIS NORMAL TO PLASMA FLOW VECTOR AND GRID EXTERNAL

Test Conditions

a. Plasma at constant density switched on and off
b. Ion grid voltages of +15V supplied by external source
c. HV on
d. Grid #4 is shorted, number of grids correspond to Fig. Page.

Test No.	Vacuum Pressure (mm/Hg)	Plasma or Flux particles cm^2/second	Grid Voltages	UV Source	Comments
1	8.0×10^{-6}	none	#1-9, +15V	off	Very quiet system
2	1.8×10^{-6}	none	#1-9, +15V	on	Visible light varified a change in intensity from Test 1
3	3.8×10^{-5}	I+ 2.4×10^{11} I- 2.0×10^{12}	#1-9, +15V	off	System very quiet
4	3.8×10^{-5}	on	#1, +15V-0V	off	#1 Grid Voltage from 15V-0V at 4 steps. No appreciable change in counts.
5	3.8×10^{-5}	on	#1-9, 0V		The UV was turned on with the HV on. Counts were recorded.
6	3.8×10^{-5}	on	#2-9, 0V #1, 0-15V	off	#1 Grid Voltage from 0V-15V, then returned to 0. No appreciable counts.
7	4.2×10^{-5}	on	#1-9 5V-15V	off	No counts
8	4.2×10^{-5}	on	#1-9 0V-50V	on	No appreciable counts
9	4.2×10^{-5}	on	#9, 0V-+5V	on	Grid #9 from 0V-15V: at +50V there is a change in polarity
10	4.2×10^{-5}	on	#1-8, -15V #9, 0V	off	No counts

could be applied, as appropriate for each run. Runs were made under different conditions of plasma, UV, HV, and grid voltage levels, and the overall operation of each run was monitored by noting the output count of the instrument. A summary of the test data for this sequence is given in Table III.

The second test sequence consisted of runs made with snout grid #9 grounded to the snout, and grid #7 held at a fixed voltage (e.g. +40, +30, +20, +10, 0, -10, -20, -30, -40V) and the inner entrance grid, #8, was varied in 10 volt steps from +40 to -50 volts. The internal ion flux densities (I+) and electron current densities (I-) for each run were measured by a probe located just inside the inner entrance grid #8. A summary of the test data for this sequence is given in Table IV.

Plots of the ion flux and electron current densities versus grid voltages for each run are contained in Appendix A.

Although the graphs in Appendix A permit some deductions to be made, they do not help determine the optimum grid voltages for the instrument. The curves were drawn from data obtained from fixed probe measurements and therefore represent local conditions rather than the total fluxes required for a conclusive determination. Additional graphs of the potential fields established by the ion

TABLE IV
PHASE II, PART 2

EFFECTS OF DIFFERENT ENTRANCE GRID VOLTAGES WITH THE OPTICAL AXIS PARALLEL TO PLASMA FLOW VECTOR WITH LANGMUIR

Test Reference

a. Grids numbers refer to Fig. Page.
b. I+ = internal ion flux densities
c. I- = electron current densities
d. Grid #9 - at the outer entrance

Grid Voltages #7	Grid Voltages #8	I-	I+	All Exterior To Grid #7 I-	All Exterior To Grid #8 I+
+40V	+40V	6.4	6.6×10^{-11}		
	+30	6.2	6.3		
	+20	6.1	6.0		
	+10	6.2	6.2		
	0	5.8	6.2		
	-10	5.4	5.8		
	-20	5.0	5.0		
	-30	4.4	4.2		
	-40	4.0	4.0		
	-50	3.6×10^{-9}	4.3		
+30V	+40V	6.0×10^{-9}	6.2		
	+30	5.8	5.5		
	+20	5.7	5.1		
	+10	5.5	4.8		
	0	5.2	4.4		
	-10	4.8	3.6		
	-20	4.4	3.0		
	-30	3.8	2.8		
	-40	3.3	3.0		
	-50	3.1	3.5×10^{-11}		
+20V	+40V	5.6	4.4×10^{-11}		
	+30	5.4	3.8		
	+20	5.2	3.2		
	+10	5.2	2.4		
	0	5.3	2.6		
	-10	4.6	2.2		
	-20	4.1	1.8		
	-30	3.6	1.7		
	-40	3.3	1.9		
	-50	3.0×10^{-9}	2.2		
+10V	+40V	5.2×10^{-9}	2.8	4.6	2.0×10^{-11}
	+30	4.7	2.1	4.6	1.1
	+20	4.4	1.6	4.6	0.5
	+10	4.2	1.2	4.6	0.5
	0	4.0	1.0	5.0	1.0
	-10	3.8	0.8	5.0	1.6
	-20	3.4	1.0	4.7	2.0
	-30	3.1	1.3	4.4	3.3
	-40	3.0	1.6	4.0	3.8
	-50	2.8	2.7×10^{-11}	3.4×10^{-11}	4.0
0V	+40V	4.8	1.5×10^{-11}	4.3×10^{-9}	1.6
	+30	4.6	1.5	4.0	1.1
	+20	4.6	1.1	3.8	0.8
	+10	4.6	0.6	3.6	1.0
	0	4.5	0.3	3.9	1.6
	-10	4.9	0.6	4.5	2.0
	-20	4.6	1.2	4.2	3.2
	-30	4.4	1.6	3.9	3.2
	-40	4.0	2.0	3.4	3.5
	-50	2.5×10^{-9}	2.7	2.8	3.7×10^{-11}

Grid Voltages #7	Grid Voltages #8	I-	I+	All Exterior To Grid #7 I-	All Exterior To Grid #8 I+	Grid #8 After 15 Minutes I+
-10V	+40V	4.2×10^{-9}	1.6	3.9	*1.5×10^{-11}	*1.3×10^{-11}
	+30	4.0	1.0	3.8	0.8	0.8
	+20	3.8	0.5	3.8	0.25	0.3
	+10	3.6	0.6	3.8	0.15	2.0×10^{-12}
	0	4.0	1.0	4.4	0.4	5.0×10^{-12}
	-10	4.6	1.7	4.4	1.0	1.0×10^{-11}
	-20	4.8	2.5	4.1	1.5	1.7
	-30	4.6	2.8	3.7	1.8	1.9
	-40	4.0	3.2	3.3	2.0	2.1
	-50	3.4	3.5×10^{-11}	2.7×10^{-9}	2.3	2.3
-20V	+40V	4.5	1.7×10^{-11}	3.6	1.8	
	+30	4.4	1.0	3.4	1.2	
	+20	4.4	0.6	3.2	0.9 - 1.0	
	+10	4.4	0.5	3.1	1.0	
	0	5.0	1.0	3.4	1.4	
	-10	5.2	1.9	3.8	1.9	
	-20	5.2	2.5	3.8	2.1	
	-30	5.0	3.6	3.4	2.7	
	-40	4.4	3.9		2.9	
	-50	3.7×10^{-9}	4.0	3.0	2.9×10^{-11}	
-30V	+40V	4.2×10^{-9}	2.4			
	+30	4.0	2.0			
	+20	3.8	1.6			
	+10	3.8	1.6			
	0	4.0	2.4			
	-10	4.4	2.9			
	-20	4.4	3.4			
	-30	4.3	4.6			
	-40	4.0	5.1			
	-50	3.4	4.7×10^{-11}			
-40V	+40V	4.6	3.1×10^{-11}			
	+30	4.4	2.4			
	+20	4.4	1.9			
	+10	4.7	2.0			
	0	4.6	2.4			
	-10	4.6	3.0			
	-20	4.5	3.9			
	-30	4.2	5.3			
	-40	4.0	6.0			
	-50	3.6×10^{-9}	8.5			

grids are found in Appendix B and the tendency of these fields is to focus the flux on or off a particular probe.

One conclusion to be drawn from the graphs in Appendix A is that the ion grids have little effect upon the number of ions or electrons that enter the instrument. The probe nearest the photomultiplier shows that the electron current varies by no more than a factor of two over a range of grid voltage varying from +50 to -50 volts.

4.2.2 TEST SEQUENCE WITH OPTICAL AXIS OF INSTRUMENT NORMAL TO THE PLASMA FLOW VECTOR

This test sequence is sometimes referred to as the Grid Current Absorption Tests because the total current drawn by the entrance grids (grids #7 and #8) was monitored and recorded as a function of the grid voltage. For test purposes grids #7 and #8 were connected to independent external DC voltages. Runs were made in which inner entrance grid #8 was held at a fixed voltage in the range from -50 volts to +50 volts, while the outer entrance grid, #7, was varied in 10 volt steps from +50 to -50 volts. The conditions of plasma, ultraviolet excitation, and HV, were varied on different runs. Probe measurements were made on each run by use of internal probes #1 and #2 in Figure 5 .

The test sequence used the following procedure:
1) After 5 hours at a pressure of 5×10^{-5} mm Hg, turn on the UV source and check the output count of the in-

strument to ensure that the system is functioning properly.

2) Turn the UV source off and the plasma source on.

3) Make a run with the plasma energy distribution peak at the maximum available level and plot a graph of the run.

4) Make runs by holding the inner entrance grid at a fixed voltage (e.g. +50V, +40, +30, +20, +10, 0, -10, -20, -30, -40, -50V)while the outer entrance grid #8 is varied in 10 volt steps from +50 to -50 volts. (Note: The mirror ring is disconnected for these runs.)

5) Record the ion flux density and the electron current density measured by probes #1 and #2.

6) Record the total currents of grids #7 and #8 combined.

7) After completing the runs in step #4 determine the optimum positive grid potential (i.e., the potential which produces the minimum total current in grids #7 and #8).

8) Connect all grids and mirror ring, #4, to the optimum positive grid potential determined in step #7.

9) Make runs with grids at optimum positive grid potential and with the ion and electron plasma densities the same as those recorded in step #5.

10) Connect all grids and mirror ring #4 to +15V (i.e., voltage normally used in flight configuration) and repeat runs in step #9.

11) Turn all power off. Wait for a few minutes and then

energize grids and HV suddenly with all grids at both optimum grid potential and at +15 volts.

A summary of the data for this test sequence steps 1-7 is given in Table V.

A typical plot of the graph obtained from step #3 is shown as the first sheet of Appendix C. This graph was plotted by D. R. Burrowbridge of Goddard Space Flight Center using currents measured with a Langmuir probe during the tests. Data obtained from the runs in step #4 plotted on the remaining sheets of Appendix C.

A comparison between the curves obtained in steps #4 and #5 show that the total grid current flow in the entrance grids follows the trend of the current measured with the Langmuir probe. The total grid current decreased significantly only when the inner entrance grid #8 was biased at the highest positive potential (i.e., +50 volts). This decrease in total grid current depended more on the value of the outer entrance grid voltage than the inner entrance grid bias.

The plasma densities measured by probe #1 and probe #2 in step #5 varied only slightly throughout the sequence. The ion flux densities measured by each probe were approximately 13×10^{-10} amp/cm^2.

TABLE V

PHASE III

VOLTAGE CONFIGURATION OF ION GRIDS WITH OPTICAL AXIS OF INSTRUMENT PARALLEL TO PLASMA FLOW VECTOR AND WITH FARADAY CUP AT APERTURE

Grid Voltages		Probe 1		Probe 2		Internal Grids	External Grids
Int.	Ext.	I+	I-	I+	I-		
+50V	+50V	7.0×10^{-12}	12.5×10^{-11}	7.0×10^{-12}	9.5×10^{-11}	3.7×10^{-8}	2.8×10^{-7}
	+40	6.5	12.5	7.0	9.5	3.7	2.25
	+30	6.0	12.5	7.0	9.5	3.8	1.5
	+20	6.0	13.0	7.0	9.5	4.8	.75
	+10	7.0	13.5	7.0	9.8	4.8	.25
	0	7.0	14.0	7.0	9.5	7.2	.05
	-10	7.0	16.5	7.0	11.5	6.2	
	-20	7.0	17.0	7.0	12.0	5.6	1.7
	-30	7.0	16.0	8.0	13.0	5.2	3.0
	-40	7.0	12.0	8.0	13.0	5.0	4.0
	-50	7.0	7.0	10.0	12.5	5.0	5.2
+40V	+50V	7.0×10^{-12}	14.0×10^{-11}	7.5×10^{-12}	10.0×10^{-11}	3.0×10^{-8}	26.0×10^{-6}
	+40	6.5	14.0	7.5	10.0	3.0	21.0
	+30	6.5	14.0	7.5	10.0	2.9	14.0
	+20	6.5	14.0	7.5	10.0	2.9	6.5
	+10	6.5	14.0	7.5	10.5	3.2	2.0
	0	6.5	14.0	7.5	11.0	3.6	7.0×10^{-7}
	-10	6.5	14.0	7.5	12.0	3.8	1.6×10^{-7}
	-20	6.5	14.0	7.5	12.5	3.4	1.0×10^{-7}
	-30	6.5	14.0	7.5	13.0	2.9	2.0×10^{-7}
	-40	6.5	12.0	7.5	13.0	2.5	3.2×10^{-7}
	-50	6.5	8.0	8.0	13.0	2.4	4.2×10^{-7}
+30V	+50V	1.2×10^{-9}	1.25×10^{-10}	1.4×10^{-11}	1.1×10^{-10}	3.6×10^{-8}	26.0×10^{-6}
	+40	1.2	1.25	1.4	1.1	3.6	20.0
	+30	1.3	1.25	1.4	1.1	3.8	14.0
	+20	1.3	1.25	1.1	1.1	4.2	6.5
	+10	1.3	1.3	1.4	1.2	4.8	2.0×10^{-6}
	0	1.3	1.5	1.3	1.2	4.6	5.0×10^{-7}
	-10	1.3	1.5	1.3	1.2	3.8	$.9 \times 10^{-7}$
	-20	1.3	1.6	1.3	1.2	3.4	1.1×10^{-7}
	-30	1.3	1.4	1.3	1.3	3.4	2.8×10^{-7}
	-40	1.3×10^{-11}	1.0	1.3	1.4	3.0	3.5×10^{-7}
	-50	1.3×10^{-11}	..7	1.3	1.4	3.0	4.5×10^{-7}
+20V	+50V	1.4×10^{-11}	11.5×10^{-11}	1.3×10^{-11}	1.1×10^{-10}	3.0×10^{-8}	26.0×10^{-6}
	+40	1.4	11.0	1.3	1.1	3.0	20.0
	+30	1.4	11.0	1.3	1.1	3.0	14.0
	+20	1.3	11.0	1.3	1.1	3.0	9.0
	+10	1.3	11.0	1.3	1.1	3.2	3.0
	0	1.3	11.0	1.3	1.1	3.2	1.0
	-10	1.3	11.0	1.3	1.2	3.4	1.5×10^{-7}
	-20	1.3	12.0	1.4	1.3	3.6	8.0×10^{-8}
	-30	1.3	13.0	1.4	1.4	3.7	1.8×10^{-7}
	-40	1.3	8.5	1.4	1.4	3.7	3.0×10^{-7}
	-50	1.3	5.0	1.4	1.4	3.4	4.4×10^{-7}
+10V	+50V	1.3×10^{-11}	1.3×10^{-10}	1.2×10^{-11}	1.3×10^{-10}	3.0×10^{-8}	28.0×10^{-6}
	+40	1.3	1.3	1.2	1.3	3.0	23.0
	+30	1.2	1.3	1.2	1.3	3.0	14.0
	+20	1.2	1.3	1.3	1.3	3.0	7.0
	+10	1.2	1.4	1.3	1.3	3.0	2.0
	0	1.2	1.5	1.3	1.3	3.0	5.0
	-10	1.2	1.4	1.3	1.3	3.0	6.0×10^{-8}
	-20	1.2	1.4	1.3	1.4	3.0	1.3×10^{-7}
	-30	1.2	1.0	1.3	1.5	3.0	2.7×10^{-7}
	-40	1.2	.7	1.3	1.5	3.0	3.5×10^{-7}
	-50	1.2	5.2	1.4	1.5	3.0	4.4×10^{-7}
0V	+50V	1.0×10^{-11}	1.2×10^{-10}	1.2×10^{-11}	1.3×10^{-10}	2.0×10^{-8}	27.0×10^{-6}
	+40	1.0	1.1	1.2	1.3	2.0	21.0
	+30	1.1	1.1	1.2	1.3	2.0	15.0
	+20	1.1	1.1	1.2	1.3	2.0	9.0
	+10	1.1	1.1	1.2	1.3	2.0	3.0×10^{-6}
	0	1.1	9.5×10^{-11}	1.2	1.3	2.0	1.0×10^{-6}
	-10	1.1	9.5×10^{-11}	1.2	1.3	2.0	2.1×10^{-7}
	-20	1.1	1.0×10^{-10}	1.2	1.4	2.0	9.0×10^{-8}
	-30	1.1	1.1×10^{-10}	1.2	1.5	2.0	1.6×10^{-7}
	-40	1.1	9.4×10^{-11}	1.3	1.5	3.0	3.0×10^{-7}
	-50	1.2	5.5×10^{-11}	1.3	1.5	3.0	4.4×10^{-7}

Grid Voltages		Probe 1		Probe 2		Internal Grids	External Grids
Int.	Ext.	I+	I-	I+	I-		
-10V	+50V	1.0×10^{-11}	1.15×10^{-10}	1.1×10^{-11}	1.3×10^{-10}	3.0×10^{-10}	28.0×10^{-6}
	+40	1.0	1.1	1.1	1.3	7.0	20.0
	+30	1.1	1.1	1.3	7.0	7.0	15.0
	+20	1.1	1.0	1.1	1.3	4.0	9.0
	+10	1.1	1.0	1.1	1.3	1.5	3.0
	0	1.1	1.0	1.1	1.3	2.3	1.2×10^{-6}
	-10	1.1	1.0	1.1	1.3	4.0	7.0×10^{-7}
	-20	1.1	1.0	1.1	1.4	1.0×10^{-9}	9.0×10^{-8}
	-30	1.1	1.1	1.2	1.4	1.5×10^{-9}	1.8×10^{-7}
	-40	1.1	1.1	1.2	1.5	3.0×10^{-9}	1.8×10^{-7}
	-50	1.1	.5	1.2	1.5	3.4	4.5×10^{-7}
-20V	+50V	1.0×10^{-11}	1.0×10^{-10}	1.1×10^{-11}	1.3×10^{-10}	1.5×10^{-9}	28.0×10^{-6}
	+40	1.0	1.0	1.1	1.2	3.2	21.0
	+30	1.0	.9	1.1	1.2	2.0	15.0
	+20	1.0	.9	1.1	1.2	1.0	10.0
	+10	1.0	.85	1.1	1.2	1.4	3.0
	0	1.1	.8	1.1	1.2	1.7	1.0
	-10	1.1	.8	1.1	1.2	1.5	2.5×10^{-7}
	-20	1.1	.85	1.1	1.2	1.0	3.0×10^{-8}
	-30	1.1	.9	1.1	1.3	8.0×10^{-10}	2.0×10^{-7}
	-40	1.1	.65	1.1	1.4	4.0×10^{-10}	3.4×10^{-7}
	-50	1.1	.45	1.1	1.5	3.0×10^{-10}	4.6×10^{-7}
-30V	+50V	1.0×10^{-11}	$.9 \times 10^{-10}$	1.1×10^{-11}	1.4×10^{-10}	2.6×10^{-9}	28.0×10^{-6}
	+40	.9	.9	1.1	1.4	2.4	21.0
	+30	.9	.85	1.1	1.3	2.3	16.0
	+20	.9	.8	1.1	1.2	2.3	10.0
	+10	.9	.75	1.1	1.2	2.4	3.5
	0	.9	.7	1.1	1.2	2.9	1.0
	-10	.9	.65	1.1	1.2	2.9	2.3×10^{-7}
	-20	.9	.65	1.1	1.2	2.7	6.0×10^{-8}
	-30	.9	.7	1.1	1.2	2.7	2.0×10^{-7}
	-40	.9	.5	1.2	1.2	2.7	3.4×10^{-7}
	-50	.9	.4	1.1	1.2	1.9	5.0×10^{-7}
-40V	+50V	$.9 \times 10^{-11}$	$.85 \times 10^{-10}$	1.0×10^{-11}	1.2×10^{-10}	3.0×10^{-9}	30.0×10^{-6}
	+40	1.0	.8	1.0	1.2	2.9	22.0
	+30	.9	.8	1.0	1.2	2.8	16.0
	+20	.9	.75	1.0	1.2	2.7	3.2
	+10	.9	.7	1.0	1.2	2.9	8.0×10^{-7}
	0	.9	.6	1.0	1.2	3.2	1.0×10^{-6}
	-10	1.0	.6	1.0	1.2	3.4	2.2×10^{-7}
	-20	1.0	.5	1.0	1.2	3.4	6.0×10^{-8}
	-30	1.0	.45	1.0	1.2	3.4	1.8×10^{-7}
	-40	1.0	.4	1.0	1.2	3.0	3.2×10^{-7}
	-50	1.0	.3	1.0	1.4	3.0	4.6×10^{-7}
-50V	+50V	1.0×10^{-11}	$.75 \times 10^{-10}$	1.0×10^{-11}	1.3×10^{-10}	4.0×10^{-9}	29.0×10^{-6}
	+40	1.0	.7	1.0	1.2	3.8	23.0
	+30	.9	.65	1.0	1.2	3.6	16.0
	+20	.9	.6	1.0	1.2	3.4	8.0
	+10	.9	.55	1.0	1.2	3.8	2.2
	0	.9	.5	1.0	1.2	4.4	5.8×10^{-7}
	-10	.9	.45	1.0	1.2	4.4	8.4×10^{-8}
	-20	.9	.35	1.0	1.2	4.4	2.1×10^{-7}
	-30	.9	.3	1.0	1.2	4.4	2.5×10^{-7}
	-40	.9	.3	1.0	1.2	4.8	3.2×10^{-7}
	-50	.9	.3	1.0	1.2	4.4	4.4×10^{-7}

4.3 PHASE III - INFLUENCE OF SNOUT GRID #9 ON PLASMA REDUCTION

The objective of Phase III was to investigate how the snout grid (cf. Figure 4) effected the reduction of plasma inside the instrument. The instrument used in this phase differed from the flight configuration tested in Phase I by the addition of the snout grid and the Faraday cup inside the entrance aperture. Probe #1 was also shifted from the position shown in Figure 5 to a location near the entrance aperture. The Faraday cup and probe #1 were used to measure the ion flux and electron current densities just inside the entrance aperture. Since the Faraday cup blocked off the entrance aperture, no UV radiation input was applied. Another difference from the flight configuration was that all grids except grids #7, #8, and #9 were disconnected from their voltage supplies. In one test sequence, grid #7 and grid #8 were each connected to separate external voltage supplies and grid #9 was grounded. In a second sequence, grids #7 and #8 were connected to the same external voltage supply and grid #9 to another. Ion grid connectors #1 and #2 in Figure 4a were used to furnish the external voltages to the instrument. All tests in Phase III were conducted with the optical axis of the instrument pointed parallel to the plasma flow vector (cf. Figure 6).

Phase III consisted of test runs made with grids #7, #8, and #9 connected in the different voltage configurations listed in Table VI. In all runs, the vacuum

TABLE VI

PHASE III - TYPICAL EXTERNAL ION FLUX AND ELECTRON CURRENT DENSITIES FOR VARIOUS PLASMA SOURCE SETTINGS

Test Conditions: Pressure 2.6×10^{-5}

FIRST SEQUENCE

Grids	#7	#8	#9	#7		#8		#9	
	Voltages			I+	I-	I+	I-	I+	I-
	+20V	+20V	0V	7.4×10^{-8}		6.2×10^{-8}		0	
		+15V	0	9.0×10^{-8}		5.2×10^{-8}		0	
		0	0	9.0×10^{-8}		3.5×10^{-8}		0	
		-15	0	8.5×10^{-8}		3.0×10^{-8}		0	
	+15	+20	0	6.2×10^{-8}		7.8×10^{-8}		0	
		+15	0	7.8×10^{-8}		6.0×10^{-8}		0	
		0	0	8.6×10^{-8}		3.6×10^{-8}		0	
		-15	0	8.0×10^{-8}		3.0×10^{-8}		0	
	0	+20	0	4.0×10^{-8}		8.0×10^{-8}		0	
		+15	0	4.6×10^{-8}		7.2×10^{-8}		0	
		0	0	6.0×10^{-8}		4.8×10^{-8}		0	
		-15	0	6.0×10^{-8}		3.0×10^{-8}		0	
	-15	+20	0	3.0×10^{-8}		7.0×10^{-8}		0	
		+15	0	2.8×10^{-8}		6.0×10^{-8}		0	
		0	0	3.5×10^{-8}		5.0×10^{-8}		0	
		-15	0	3.0×10^{-8}		5.0×10^{-8}		0	

SECOND SEQUENCE

Grids	#7 & #8	#9	7 & 8		9		7 & 8		9	
	Voltages		I+	I-	I+	I-	I+	I-	I+	I-
	+20V	+20V	1.0×10^{-7}		2.4×10^{-5}		8.0×10^{-8}		2.7×10^{-6}	
		+15	1.2×10^{-7}		1.5×10^{-5}		9.0×10^{-8}		2.1×10^{-6}	
		0	3.0×10^{-7}		2.7×10^{-5}		8.0×10^{-8}		6.0×10^{-6}	
		-15	4.0×10^{-7}			2×10^{-7}	1.0×10^{-7}		4.5×10^{-7}	
	0	+20	6.8×10^{-8}		1.6×10^{-5}		5.4×10^{-8}		2.4×10^{-5}	
		+15	7.0×10^{-8}		2.7×10^{-6}		5.0×10^{-8}		1.9×10^{-5}	
		0	1.9×10^{-7}				6.0×10^{-8}		5.0×10^{-6}	
		-15	1.9×10^{-7}			1.2×10^{-7}	6.0×10^{-8}		5.0×10^{-7}	
	-15	+20	3.4×10^{-8}		2.2×10^{-5}		3.5×10^{-8}		2.6×10^{-6}	
		+15	4.0×10^{-8}		6.0×10^{-8}		3.0×10^{-8}		1.8×10^{-6}	
		0	3.0×10^{-8}		2.8×10^{-6}		3.2×10^{-8}		5.0×10^{-6}	
		-15	3.0×10^{-8}		2.0×10^{-8}		3.0×10^{-8}		5.0×10^{-7}	

chamber pressure was maintained at 2.6×10^{-5} mm Hg. A run was made for each voltage configuration by varying the plasma energy distribution peak in steps throughout its available range. Typical densities of flux and electron current densities produced for each voltage setting are listed in Table VI. The two sequences of runs made during Phase III are described in Sections 4.3.1 and 4.3.2.

4.3.1 TEST SEQUENCE WITH SNOUT GRID #9 GROUNDED

Runs were made for each of the voltage configurations listed in Table V. Graphs showing the variation of ion flux densities and electron current densities for each voltage configuration are contained in Appendices D and E respectively.

The upper graph in Appendix D represents the number of ions injected towards the instrument as a function of the plasma source settings, i.e., the external ion flux densities (I ion) in Table VI. All other graphs in Appendix D show the trends of the ion flux densities measured inside the dust cover for various voltage configurations. In all except two cases, the ion density inside the dust cover is essentially constant for all plasma levels and depends upon the voltage on outer entrance grid #7. When both grids were negative and when one grid was zero, and the other negative. The ion density inside the dust cover became approximately one order of magnitude

less than the injected ion density at all source settings.

The format for presenting the electron density curves in Appendix E is the same as that used above for Appendix D. Note that the trend of all distribution curves of electron density is the same for all internal grid #8 voltages and is not appreciably affected by different outer grid #7 voltages. Note also that the electron energy distribution inside the dust cover is approximately three orders of magnitude less than the energy distribution of the injected electrons.

4.3.2 TEST SEQUENCE WITH GRID #9 SUPPLIED WITH DIFFERENT VOLTAGES

For this test sequence runs were made at each of the voltage configurations listed in Table V. Graphs showing the variation of ion flux densities and electron current densities for each voltage configuration are contained in Appendices F and G. The format for presenting the curves in these appendices is the same as that used in Section 4.3.1. Note that all curves show approximately the same trend as the corresponding curves in Appendixes D and E. A point of interest in Appendix F is that positive snout grid #9 potentials (i.e., +20 and +15 volts) cause the levels of ion density inside the dust cover to be approximately two orders of magnitude less than the level of injected ion density. This reduction is approxi-

mately one order of magnitude more than the corresponding decrease attained in Appendix E with the snout grid grounded.

4.3.3 DISCUSSION OF PHASE II RESULTS

The Phase III tests showed that snout grid #9 was capable of varying the ion flux that entered the instrument. When positive voltages were applied to this grid, the ion densities inside the instrument became less by one order of magnitude than when negative voltages were applied (cf. Appendix F). However, a snout grid would reduce the UV input level and thus would lessen the ability to collect data. Moreover, because other tests showed that an orbital plasma environment did not induce any appreciable deterioration, the addition of a snout grid for plasma reduction is not considered necessary.

The results of Phase III tests also showed that the grid voltages that provided the best electron rejection did not provide the best ion rejection and vice versa.

Phase III tests also showed that the magnitude of the grid voltages had little effect upon the electron current densities inside the dust cover, and that an electron energy distribution inside the dust cover approximated that outside the instrument (cf. Appendices E and G).

Nevertheless, not all the results obtained from Phase III supported the conclusion that positive ion grid voltages (such as those used in the OSO-D) tend to reject positive ions and accelerate electrons. A possible explanation is that the Phase III results depended upon plasma level measurements and that the devices used for these measurements were limited to local flux phenomena and did not include total fluxes (cf. section 4.2.1), which were not measured.

4.4 PHASE IV - EFFECT OF INCIDENT PLASMA ON RESPONSE OF DETECTION SYSTEM WITH NO DUST COVERS INSTALLED

Phase IV studied how incident plasma affected the response of a detection system when operating without the immunity normally offered by the dust covers and the ion grids. Tests were conducted with the optical axis of the instrument directed normal to the plasma flow vector with the dust covers removed and with no voltage on the ion grids. Obviously these conditions are worse than any that would be encountered in the actual operation of the instrument.

Test runs were made at different plasma levels and the output count of the detection system was recorded for each run. The plasma level was increased for successive runs until it reached the maximum.

Test data for each run are listed in Table VII. Note that output corresponding to approximately 10^4 pulses per second was obtained and that no HV discharge was observed even when the run was continued for one half hour at the maximum level of available plasma.

When the above test sequence was completed, the dust covers were replaced and the instrument was reoriented in the test chamber so that its optical axis was parallel to the plasma flow vector and pointed at the UV source. In this configuration the instrument performed satisfactorily.

4.4.1 DISCUSSION OF PHASE IV RESULTS

The results summarized in Table VII show that no HV discharge was produced when maximum plasma energy and number of particles were applied to an instrument without dust covers but that the output of the instrument contained an unacceptably high noise count. The results also indicated that an approximately linear relationship existed between the output count of the detection system and the applied plasma density. This relationship was demonstrated by increasing the plasma density by a fixed amount and noting that the output counts increased proportionately. As expected, the detection system is not immune to directly impinging plasma, but it is well protected by the dust covers and ion grids in the present flight configuration of the instrument.

TABLE VII

TEST DATA
PHASE FOUR WITH OPTICAL AXIS OF INSTRUMENT ORIENTED NORMAL
TO PLASMA FLOW VECTOR WITH NO DUST COVERS OR SCREENS

Test No.	Plasma Level	Retarding Potential	I+	I-
I	On	0	1.2×10^{-8}	$.260 \times 10^{-6}$
		1	1.2	.255
		2	1.2	.255
		3	1.2	.270
		4	1.25	.270
		5	1.25	.275
		6	1.25	.275
		7	1.25	.275
		8	1.25	.275
		9	1.25	.280
		10	1.25	.250
		12	1.2	.225
		14	1.2	.195
		16	1.2	.165
		18	1.15	.140
		20	1.15	.120
		25	1.1	.085
		30	1.1	.066
II	Twice the Level of Test I	0	1.8×10^{-8}	5.0×10^{-7}
		1	1.9	5.2
		2	1.95	5.3
		3	2.0	5.4
		4	2.05	5.4
		5	2.1	5.3
		6	2.1	5.2
		7	2.1	5.1
		8	2.15	5.0
		9	2.15	4.8
		10	2.20	4.6
		12	2.20	4.2
		14	2.20	3.7
		16	2.15	3.3
		18	2.15	2.9
		20	2.15	2.6
		25	2.10	2.0
		30	2.10	1.6
III	Twice the Level of Test II	0	4.0×10^{-8}	7.4×10^{-7}
		1	4.4	7.6
		2	4.6	7.7
		3	4.8	7.8
		4		7.9
		5		8.0
		6		8.0
		7		8.0
		8	4.8	7.9
		9		7.8
		10		7.6
		12		6.8
		14		5.7
		16		4.7
		18		3.9
		20	4.6	3.2
		22		
		25		2.2
		30	4.4	1.8

Test No.	Plasma Level	Retarding Potential	I+	I-
IV	Twice the Level of Test III	0	8.0×10^{-8}	11.0×10^{-7}
		1	8.0	11.5
		2	7.8	12
		3	7.6	12
		4	7.5	12
		5	7.5	12
		6	7.6	12
		7	7.6	12
		8	7.6	12
		9	7.7	11
		10	7.7	11
		12	7.8	9.5
		14	7.7	8.1
		16	7.7	6.6
		18	7.6	5.4
		20	7.6	4.4
		25	7.4	3.1
		30	7.2	2.5
		35	7.0	
V	Twice the Level of Test IV	0		2.1×10^{-7}
		1	same as	21.5
		2	Test IV	22
		3		22
		4		22
		5		22
		6		22
		7		22
		8		22
		9		21.5
		10		21
		12		20.5
		14		20
		16		19
		18		18
		20		16.5
		25		13
		30		10
VI	At Highest Possible Level	All	9.0×10^{-8}	1.2×10^{-6}

5.0 CONCLUSIONS

The following conclusions were derived from a study of the results obtained in the orbital plasma tests:

1) Orbital plasma does not introduce any high-voltage discharge during the operation of the HCO experiment of the OSO-D.

2) The performance of the flight configuration (i.e., with dust covers on grid +15 volts applied to all ion grids) of the HCO experiment is essentially unaffected by the orbital plasma. Although the detection system output included a spurious short lived transient at the turn-on of the instrument, this transient was short (less than two seconds) enough to be acceptable.

3) The ion grids do not greatly affect the number of ions or electrons that enter the instrument but the dust covers provide ample protection from the effects of orbital plasma.

4) Efforts to determine an optimum grid voltage configuration gave inconclusive results and further tests are recommended. The present tests, however, confirm the expectations that an optimum grid voltage configuration would be one that produced a compromise between electron and ion rejection.

5) The ability of the flight configuration to reject plasma could be improved by installing a grounded grid outside of the snout entrance aperture. This modification

however, is not recommended because it reduces the optical efficiency of the instrument.

6.0 FUTURE EXPERIMENTS

Future experiments will be conducted to furnish more conclusive results than those obtained in some parts of these tests (cf. Sections 4.2.1 and 4.3.3). For this purpose, a test station will be established at the Harvard College Observatory for testing different designs in probable plasma environments. This station will include a plasma source modeled after the one used at GSFC for these tests. In addition, a simple model of an instrument for use as a test bed in the determination of an optimum grid configuration is being prepared.